K-0

EFFECT OF Hf-RICH PARTICLES ON THE CREEP LIFE OF A HIGH-STRENGTH NiAl SINGLE CRYSTAL ALLOY

A. Garg, S. V. Raj, and R. Darolia*

NASA Lewis Research Center, Cleveland, Ohio

*General Electric Aircraft Engines, Cincinnati, Ohio

Abstract

Additions of small amounts of Hf and Si to NiAl single crystals significantly improve their high-temperature strength and creep properties. However, if large Hf-rich dendritic particles formed during casting of the alloyed single crystals are not dissolved completely during homogenization heat treatment, a large variation in creep rupture life can occur. This behavior, observed in five samples of a Hf containing NiAl single crystal alloy tested at 1144 K under an initial stress of 241.4 MPa, is described in detail highlighting the role of interdendritic Hf-rich particles in limiting creep rupture life.

Introduction

In recent years, there has been an increased emphasis on developing NiAl-based alloys for high temperature structural applications for aircraft engines [1]. The choice of this material is due to the fact that it possesses a desirable combination of properties some of which are far better than commercial superalloys. These properties include a higher melting temperature, lower density, larger thermal conductivity, and better oxidation resistance than superalloys [1-3]. However, two limitations that have historically prevented the use of NiAl in load bearing applications are its brittleness at low temperature and poor high temperature strength. Therefore, most of the current research is focused on improving these properties.

Alloying strategies for improving the creep properties of single crystal NiAl via precipitate hardening have proved very successful. In particular, the role of Hf in improving the creep strength of NiAl has evoked great interest in recent years [1-8], and there is now considerable data which suggest that the desired strength levels can be achieved in NiAl single crystals alloyed with Hf [1-3,5,8]. Minor Hf additions in NiAl single crystals result in the precipitation of one or more of the three phases, a G-phase ($Ni_{16}Hf_6Si_7$), a Heusler phase (Ni_2AlHf) and a NiHfSi phase [6,8,9,10]. Two of these phases contain Si which is not an intentional alloying addition but is picked up from reaction with the ceramic shell mold during directional solidification of the single crystal ingots.

Tensile creep tests were performed on samples machined from a Hf containing NiAl single crystal alloy in order to quantify the creep rupture properties of these alloys for design purposes. However, it was observed that a considerable amount of scatter existed in creep rupture life of these samples. A detailed study of the failed samples was conducted using optical, scanning (SEM) and transmission electron microscopy (TEM) to understand the probable causes of the scatter and the results are reported in this paper.

Experimental

Single crystal ingots of a Hf containing NiAl alloy were grown from the melt by a modified Bridgman technique at General Electric Aircraft Engines (GEAE), Cincinnati, Ohio. The exact chemical composition of the alloy is GEAE's proprietary information. These ingots were batch homogenized in a high temperature furnace for 50 h at 1590 K, where each batch contained typically 5-10 ingots. Cylindrical specimens for tensile creep testing along <001> were machined from different ingots. Constant load creep testing was conducted in air at 1144 K under an initial stress of 241.4 MPa by Joilet Metallurgical Laboratories Inc., Illinois for GEAE. The five tested specimens, which showed a creep rupture life (t_f) varying from 37 to 343.6 h and a creep ductility (ε_f) varying from 39.9 to 11% (Table I), were chosen for detailed study. These specimens were machined from the ingots designated as A, B, C and D which were homogenized in four different batches. The number in front of an ingot (e.g. 8 in A-8) refers to the number of the specimen machined from that ingot. Based on the creep rupture life, A-8 and A-11 have been categorized as low life specimens (t_f < 50 h), C-5 as an intermediate life specimen (50 h > t_f < 300 h), and D-16 and B-17 as high life specimens (t_f > 300 h) in this paper. It is interesting to note that A-8 and A-11 were machined from the same ingot and both of these specimens showed a low creep rupture life.

Only one of the two fractured pieces of each of the five tensile specimens was available for detailed examination and analysis. Therefore, care was taken to obtain maximum information from the as-fractured specimens before using any destructive technique. First, the fracture surfaces of the failed specimens were examined in a JEOL-6100 SEM equipped with a Kevex X-ray detector. Energy dispersive spectroscopy (EDS) was utilized when necessary to obtain chemical information from different regions of the fracture surfaces. Second, morphology of the fractured specimens, shapes of the fracture surfaces, and slip traces on the sample surfaces were documented. Third, X-ray Laue patterns were obtained from the buttonhead sections of each of the five specimens to determine the extent of deviation of the tensile axis from the required <001> orientation. Having obtained these pieces of information, the specimens were mounted, ground and polished longitudinally to approximately their mid-sections for optical examination. The gage and buttonhead sections in each sample were examined in the as-polished condition and also after etching. The etchant used was a freshly prepared solution of 33 % nitric acid, 33 % acetic acid, 1 % hydrofluoric acid and 33 % water. Chemical analysis of the specimens was also conducted to ensure that the nominal chemical composition was the same for the five specimens.

Detailed TEM analysis was conducted only on the lowest (A-8) and the highest (B-17) life specimens (Table I), using a Phillips 400T transmission electron microscope. Foils for TEM were

Micromechanics of Advanced Materials:
A Symposium in Honor of Professor James Li's 70th Birthday
Edited by S.N.G. Chu, P.K. Liaw, R.J. Arsenault, K. Sadananda,
K.S. Chan, W.W. Gerberich, C.C. Chau, and T.M. Kung
The Minerals, Metals & Materials Society, 1995

Table I Tensile Creep Rupture Life and Ductility Data for a <100> NiAl (Hf) Single Crystal Alloy

Creep stress: 241.4 MPa Temperature: 1144 K

Specimen ID	Desired orientation	Deviation from <100> axis	Creep ductility, ϵ_f (%)	Rupture life, t_f (h)	
A-8	<100>	≤1.0°	39.9	37.0	Low
A-11	<100>	2.0°	34.2	49.1	
C-5	<100>	1.5°	29.8	173.4	Intermediate
D-16	<100>	≤1.0°	11.0	322.5	High
B-17	<100>	1.5°	12.3	343.6	

prepared from the longitudinal sections of the already ground specimens and thinned using typical electropolishing techniques. The electrolyte used was a solution of 70% ethanol, 14% distilled water, 10% butylcellosolve, and 6% perchloric acid cooled to 263 K. Different regions along the length of the samples from the fractured end to the buttonhead were chosen for TEM examination and the foils from each region contained the loading axis.

Results and Discussion

A SEM examination of the fracture surface of specimen A-8 revealed a mixture of elongated dimples (Fig. 1(a)), and cleavage facets (Fig. 1(b)). All other specimens failed by cleavage where different types of cleavage fracture were observed. Figure 1(c,d) shows a radial chevron and a river pattern observed on the fracture surfaces of samples C-5 and B-17, respectively. A close

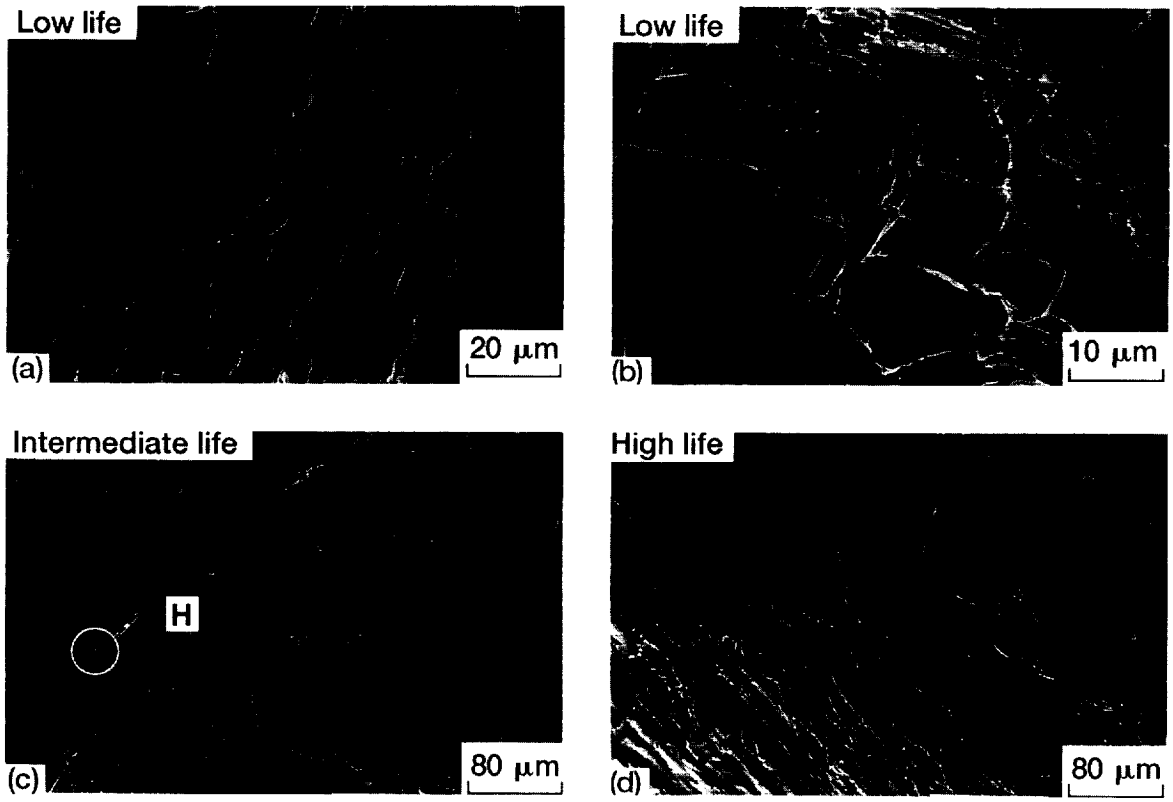

Fig. 1 SEM fractographs showing (a) elongated dimples and (b) cleavage fracture in specimen A-8, (c) radial chevron cleavage in specimen C(5), and (d) river pattern cleavage in specimen B-17. The fracture origin is marked by H in Fig. 1(c).

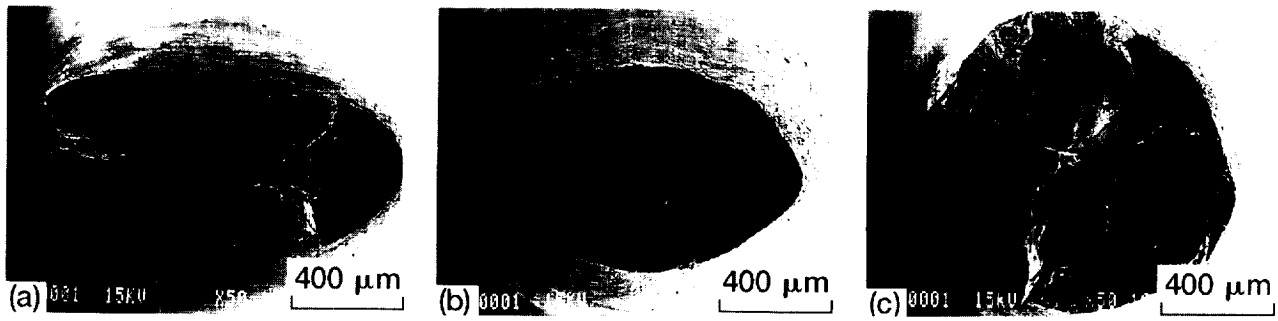

Fig. 2 Macroscopic view showing geometry of the fracture surfaces (a,b) elliptical for A-11 and C-5, respectively, and (c) circular for B-17.

examination of the fracture surface of sample C-5 revealed that the cleavage facets could be traced back to the fracture origin (marked H in Fig. 1(c)), which in this case was a large (size ~ 25 μm) particle. The EDS pattern obtained from the particle showed it to be rich in Hf and to contain some O, thereby suggesting that it was a HfO_2 particle entrapped from the melt. In all other specimens, fracture appeared to have commenced randomly since no specific fracture initiation site could be located. Casting porosity present in the specimens, and seen clearly in Fig. 1(c), did not appear to have caused final failure.

The shape of the fracture surfaces was distinctly different for the five specimens and a correlation between the fracture surface morphology and the fracture life was apparent. The geometry of the fracture-surfaces varied from an elliptical cross-section for the low and intermediate life specimens (e.g. Fig. 2(a) for A-11, and Fig. 2(b) for C-5) to a circular cross-section (e.g. Fig. 2(c) for B-17) for the high life specimens. Although all the specimens were oxidized, double slip traces were distinctly visible on the outer surface of the specimen B-17 (Fig. 3(a)). In the specimen C-5, faint traces of predominantly single slip (arrow in Fig. 3(b)) became visible only after polishing the specimen, and unfortunately, slip traces on the low life specimens could not be revealed. The X-ray Laue data from the buttonheads of the test specimens indicated that all the specimens were within 2° of the <001> orientation (Table I), and the extent of deviation showed no correlation with the fracture life.

An examination of the data in Table I indicated that the specimen with a high creep ductility had a low rupture life and vice-versa. This trend was also evident in Fig. 4(a) which is a plot of ε_f vs. t_f and shows an inverse linear correlation between the two variables. Such a correlation can be rationalized in terms of the Monkman-Grant relationship i.e. $t_f \propto 1/\dot{\varepsilon}$ [11], where a specimen creep tested at different strain rates ($\dot{\varepsilon}$) is expected to exhibit an inverse linear relationship between fracture strain and rupture life, as shown in Fig. 4(b). This suggested that the five specimens had deformed at different strain rates in spite of the fact that they were tested under identical stress and temperature conditions. Consequently, these observations and SEM results (Figs. 1-3) suggested that scatter in the creep rupture life was primarily due to factors affecting deformation behavior and only secondarily to those responsible for fracture initiation in the material.

Optical metallography was conducted on the five specimens to see if there were any macrostructural differences that could have influenced the deformation behavior. The longitudinal polished sections of the specimens were etched to observe the distribution of the precipitates in each specimen. Although the surfaces were always non-uniformly etched, the etched sections in all the specimens showed a uniform distribution of precipitates, which were later identified by TEM to be the G-phase that is expected to precipitate in Hf containing NiAl single crystals [6]. An optical micrograph showing the typical distribution of these precipitates

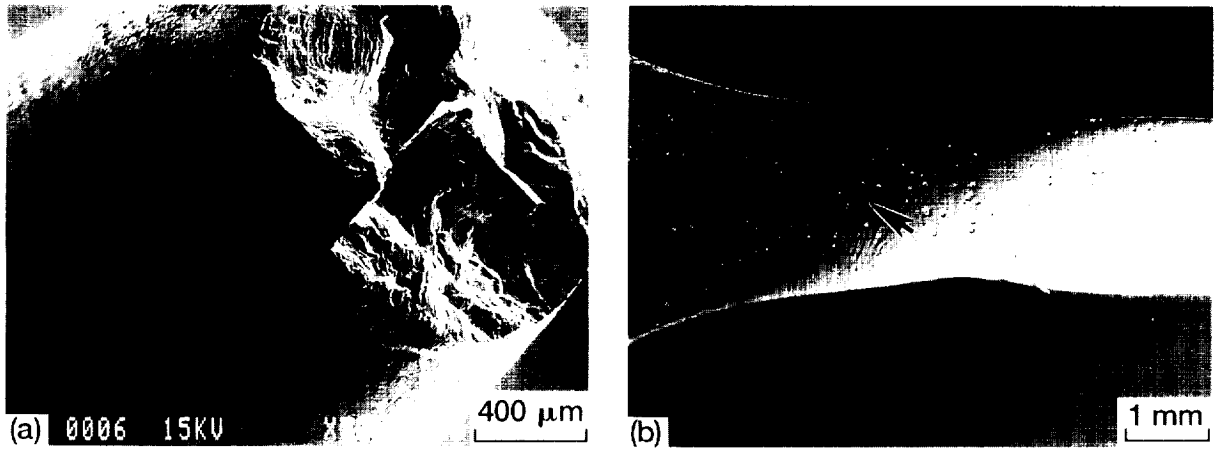

Fig. 3 (a) SEM micrograph showing double slip traces on the outer surface of specimen B-17, (b) Optical micrograph of the longitudinal polished section of specimen C-5 showing faint traces (arrow) of predominantly single slip.

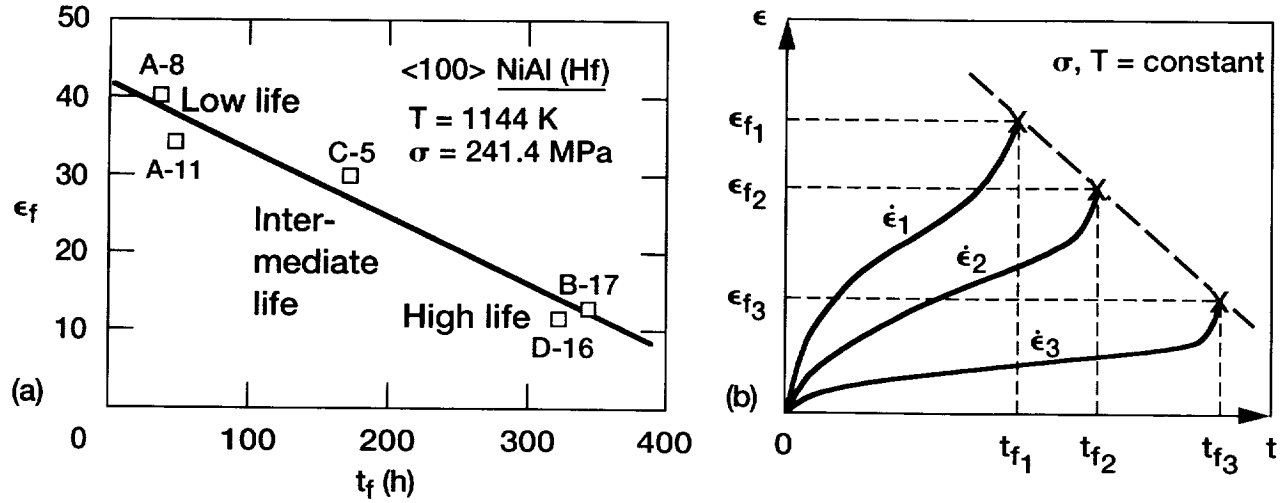

Fig. 4 The relationship between fracture life (t_f) and creep ductility (ϵ_f) for the five specimens shown in table I, (b) Expected relationship between t_f and ϵ_f for a specimen deforming at different rates and obeying Monkman-Grant relationship, $t_f \propto 1/\dot{\epsilon}_f$.

is shown in Fig. 5 for the specimen C-5. In addition to these precipitates, the occasional presence of relatively large particles was also observed in all specimens. Previous studies on similar alloys [12] suggested that these were Hf-rich particles which were formed during casting of the single crystal ingots that did not completely dissolve during the homogenization treatment. Repeated polishing and etching efforts to obtain uniformly etched surfaces were unsuccessful, and overall macrostructural differences, if any, that existed among the five specimens could not be assessed through optical microscopy.

During the course of the TEM study, described later in this paper, it was observed that the presence of large Hf-rich particles in the low life specimens had played a major role in changing the deformation behavior. Realizing that the etchant may have been ineffectve in revealing these particles in the optical microscope, ingots from which the low and high life specimens were machined were obtained from GEAE. Different sections of the ingots were ground and polished and examined in the BSE mode of SEM to observe these particles. The ingot A, from which the two low life specimens (A-8 and A-11) were machined, was found to contain a high density of large Hf-rich particles (size ~ 5-500 μm) in interdendritic regions, as shown in Fig. 6. In comparison to this, the high life ingot B was almost free of such large Hf-rich particles and only occasionally showed small particles of size ≤ 0.5 μm.

A detailed TEM study was undertaken to understand the role of these Hf-rich particles in altering the deformation behavior and to explain why samples of nominally similar composition, given the same heat treatment and creep tested under identical conditions were deforming differently. The lowest life sample, A-8, and the highest life sample, B-17, were chosen for detailed TEM analysis.

A general TEM microstructure of the buttonhead section of the low life sample, A-8, close to a $<100>_{NiAl}$ zone-axis is shown in Fig. 7(a). The microstructure consisted of a high density of fine cuboidal precipitates (size ~ 5-50 nm) which were distributed uniformly in the NiAl matrix, and some plate-shape precipitates (size ~ 100 nm) on edge-on {010}NiAl planes making a square grid type pattern (arrows in Fig. 7(a)). A selected area diffraction pattern (SADP), shown in the top right-hand corner in Fig. 7(a), showed a cube-on-cube orientation relationship between the precipitates and the matrix, and a FCC structure with lattice parameter a = 1.144 nm for the precipitate phase. This phase was identified as the G-phase, which has been reported to precipitate in NiAl single crystals containing Hf and Si [6]. The G-phase has a small misfit (1.2%) and nucleates coherently in the NiAl matrix

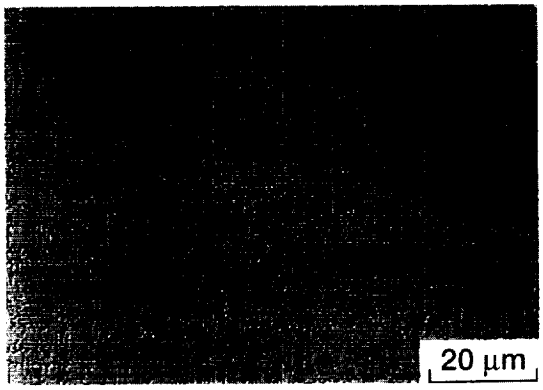

Fig. 5 Optical micrograph of an etched section of the longitudinally polished surface of specimen C-5 showing the typical distribution of G-phase precipitates in the specimens.

Fig. 6 A representative SEM micrograph showing Hf-rich dendritic particles present in different sections of the ingot A.

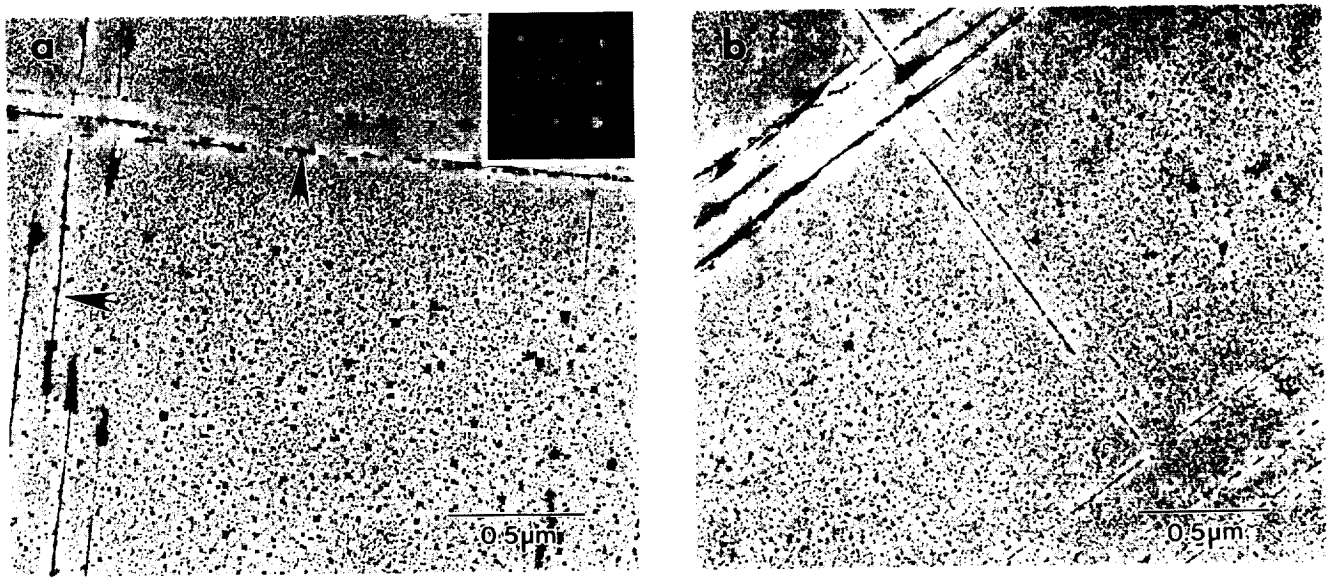

Fig. 7 TEM micrographs close to a <001> zone-axis showing general microstructure of the buttonheads for specimens (a) A-8, (b) B-17. The SADP in (a) shows a cube on cube orientation relationship between the G-phase precipitates and NiAl matrix.

(a = 0.289nm). Those precipitates which nucleate on dislocations grow at an accelerated rate, presumably due to a pipe-diffusion mechanism, and adopt a plate-shape morphology resulting in minimization of strain energy. The G-phase platelets were associated with precipitate free zones that can be clearly seen in Fig. 7(a). The general microstructure of the buttonhead section of the high life sample, B-17 (Fig. 7(b)), was essentially similar to that of the low life sample, A-8 (Fig. 7(a)). Although the two samples were exposed to 1144 K for quite different times (37 h for A-8 vs. 343.6 h for B-17), no apparent differences in the size, distribution and morphology of the G-phase precipitates in the two samples could be discerned. This suggested that the G-phase was thermally stable and had a low coarsening rate at 1144 K in this alloy.

In addition to the G-phase precipitates, Hf-rich particles were observed in the TEM foils of both the specimens. Significantly, all the foils made from the low life specimen, A-8 contained a much higher density of these particles, which were also considerably larger in size than those made from the highlife specimen, B-17. A representative micrograph showing some of these particles in the TEM foil of each of the two specimens is shown in Fig. 8(a,b), respectively. Frequently, these particles fell out during electropolishing due to preferential thinning at the particle-matrix interface leaving behind holes in the foil. This was frequently observed in the foils made from specimen A-8. These observations were consistent with the presence of a significant density of Hf-rich interdendritic particles observed by SEM in the ingot A (Fig. 6). Occasionally, a part of the Hf-rich particle that was still attached to the matrix could be seen near the hole and its edges were thin enough to obtain electron diffraction patterns. Indexing of the diffraction patterns along with the chemical information obtained from EDS identified these particles to be either the Ni_2AlHf [12] or NiHfSi phase [10]. The density of G-phase precipitates around the Hf-rich particles was found to be noticeably lower than in regions away from them, and the extent of the lower precipitate density region increased with particle size. These observations suggested that the presence of large Hf-rich particles depleted the surrounding matrix of Hf (/and Si), thereby leading to a lower density of the G-phase

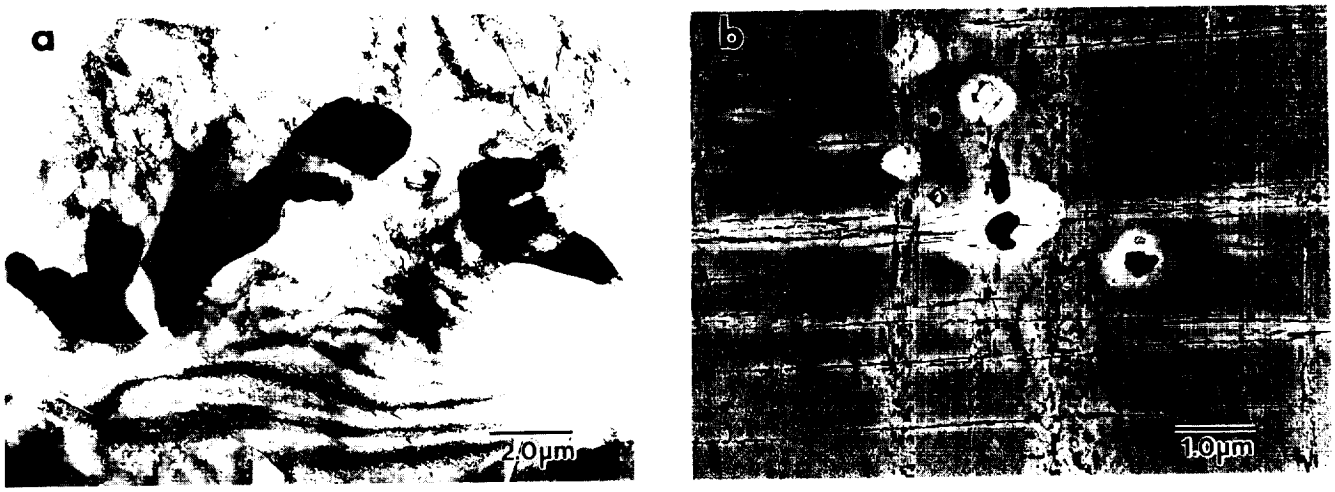

Fig. 8 Typical Hf-rich particles observed in the TEM foils of specimens (a) A-8, and (b) B-17.

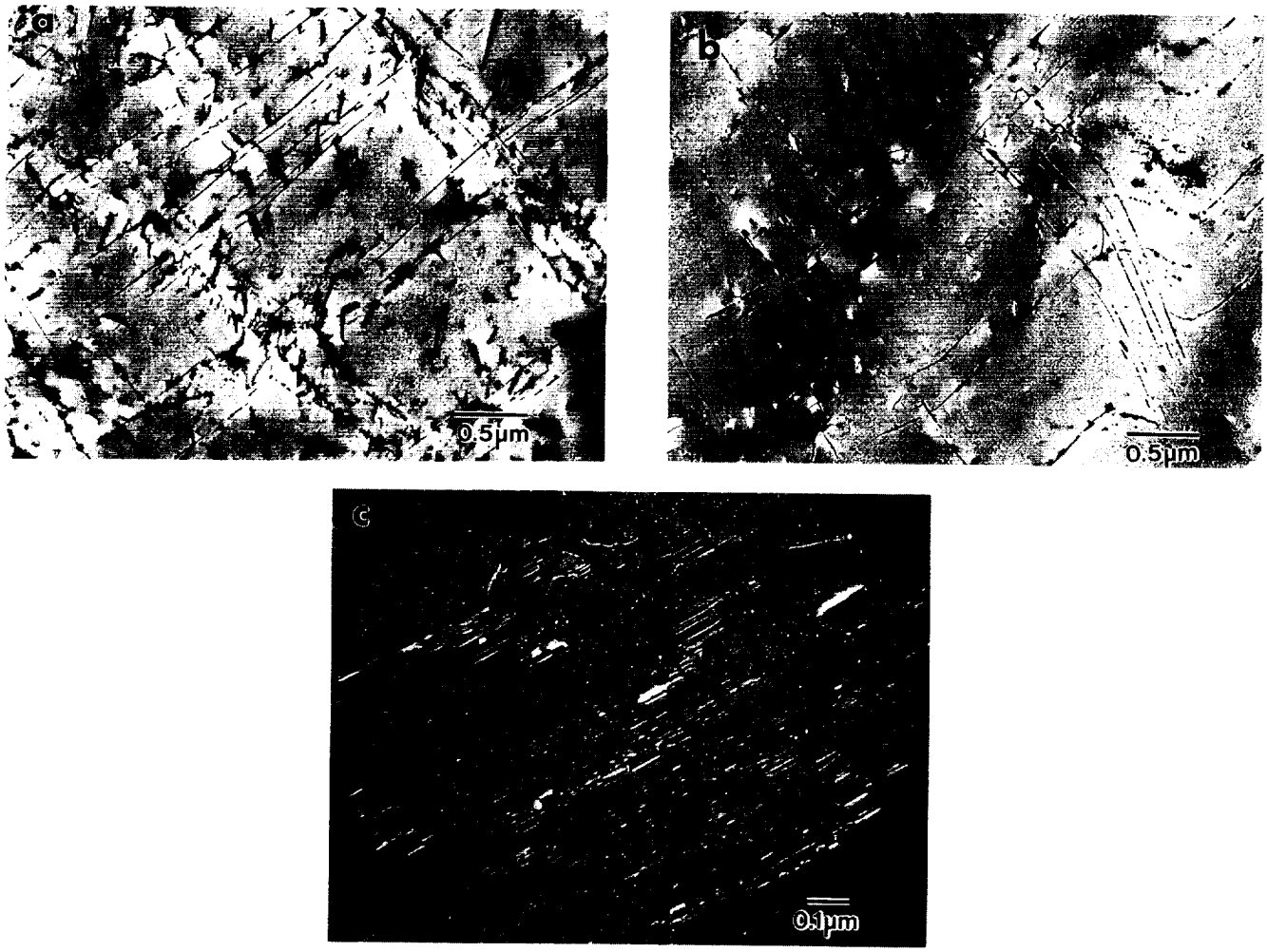

Fig. 9 Typical microstructure of the gauge section close to the fracture end in specimen (a) B-17, and (b) A-8. Multiple Orowan looping of dislocations around large G-precipitates in sample B-17 is shown in a weak-beam dark-field image in (c).

precipitates around them. Since this decrease in precipitate density corresponds to an increase in the G-precipitate spacing, the regions around Hf-rich particles are expected to be of lower strength than the rest of the matrix and, therefore, will be referred to as "soft" regions.

A comparison of the microstructure of the gage section close to the fracture end of specimens B-17 and A-8 is shown in Fig. 9(a,b), respectively. The high life specimen B-17, with a creep ductility of 12.3%, showed a uniform distribution of dislocations throughout the foil (fig. 9(a)). Extensive Orowan looping of dislocations, especially around the large G-phase precipitates, could be clearly seen in the weak-beam dark-field images taken from this specimen (Fig. 9(c)). In contrast, the low life specimen A-8 which exhibited a creep ductility of ~ 40 %, showed very few dislocations in the matrix (Fig. 9(b)). In addition, a number of deformation/shear bands were observed in this foil. A representative micrograph showing two of the shear bands is shown in Fig. 10, which is a bright-field image close to a <010> zone-axis and contains the stress axis. Assuming the stress axis to be [001] and the zone-axis to be [010], a trace analysis indicated that shear had occurred along the [101] direction. Regions of shear bands that contained the aligned G platelets showed formation of some subgrain boundaries in the precipitate free zones that surrounded the platelets. These are shown by arrows in Fig. 10.

The microstructure of the gage section away from the fracture end also exhibited a uniform distribution of dislocations in specimen B-17, similar to that shown in Fig. 9(a). This suggested that the high life specimen B-17 had deformed uniformly throughout the whole gauge section. In contrast, the gage region away from the fracture end in the specimen A-8 showed few dislocations and no deformation bands, thereby suggesting that deformation in the low life specimen A-8 was non-uniform and confined close to the fracture end.

The ideal slip mode in NiAl(Hf) single crystals tested along the [001] axis is the activation of four slip systems, $(10\bar{1})[101]$, $(101)[10\bar{1}]$, $(01\bar{1})[011]$ and $(011)[01\bar{1}]$ [13,14]. SEM observations of a circular cross-section of the fracture surface (Fig. 2(c)) and double slip traces on the specimen surface (Fig. 3(a)), and TEM observations of a uniform dislocation distribution throughout the gage section (Fig. 9(a)), suggest that the high life specimen B-17 had deformed uniformly by the activation of at least two slip systems. In contrast, SEM observations of an elliptical cross-section of the fracture surface (Fig. 2(a)), and TEM observations of a low dislocation density (Fig. 9(b)) and formation of shear bands (Fig. 10) close to the fracture surface, suggest that the low life specimen A-8 had deformed non-uniformly by predominantly single slip. These observations suggested that deviation from a double slip to a single slip

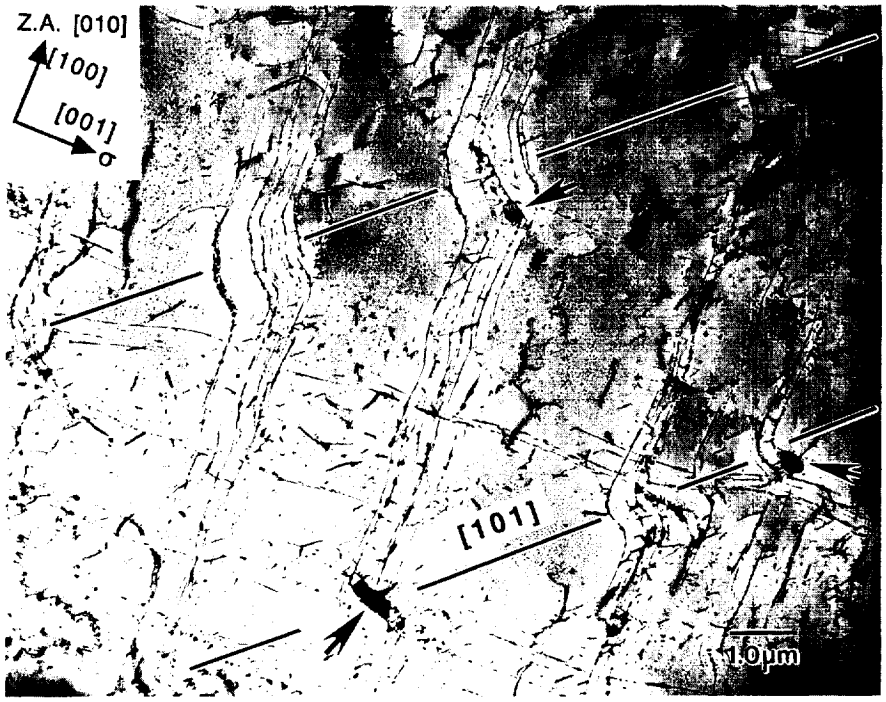

Fig. 10 Typical shear bands observed in the specimen A-8 near the fracture end.

behavior was likely responsible for lowering the creep rupture life.

An important question as to what was responsible for causing a change from a double slip to a single slip behavior still needs to be addressed. A major difference observed between the specimens A-8 and B-17 was a noticeably higher density of large (size > 0.5 μm) Hf-rich particles in the former specimen. However, SEM observations indicated that, in general, these particles were not responsible for causing final fracture. This is reasonably justified since the test temperature was above the brittle to ductile transition temperature of the alloy [3,14], and even if the cracks originated from any of these particles, matrix plasticity is expected to be sufficient to prevent their propagation to final fracture (except for specimen C-5). However, if these particles influenced the plasticity of the matrix in any way, they could have contributed towards a change in the slip behavior. Therefore, it was decided to focus the TEM examination around these particles.

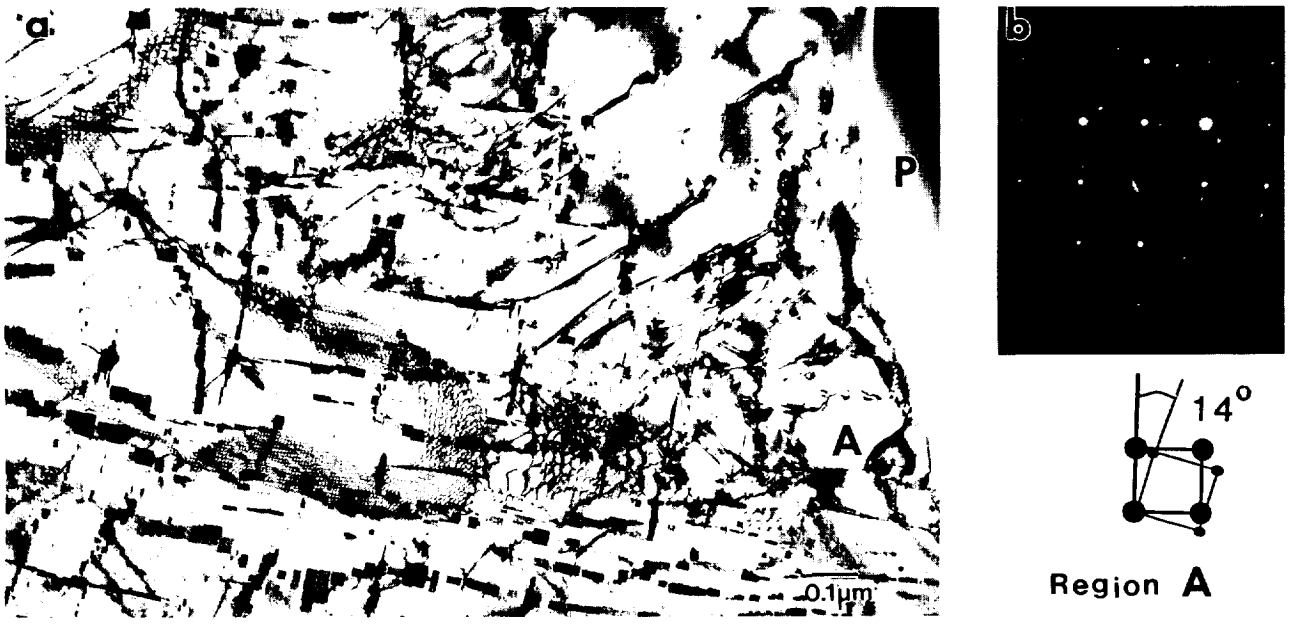

Fig. 11 (a) General microstructure in a section around a Hf-rich particle observed in a foil close to the fracture end in specimen A-8. Only a part of the etched out particle is shown and is marked by P. (b) A SADP close to region A in (a) showing a misorientation of 14 ° between the subgrains.

Fig. 12 Emission of slip bands (arrows) from two Hf-rich particles, marked P, in the specimen A-8.

Hf-rich particles were generally observed in relatively thicker sections of the foil. Nevertheless, it was clear that the microstructure around these particles was very different from that observed in regions away from the particles. Figure 11(a) shows a representative microstructure in a section of the region around a Hf-rich particle present near the fracture end of specimen A-8. This particle had fallen out of the foil during electropolishing and only a part of the corresponding etched out region, marked as P, is shown in the micrograph. A large number of subgrains and dislocation networks were observed in the soft region around the particle, thereby suggesting that intense deformation had occurred in this region. This was typical of the microstructures around all the Hf-rich particles that could be observed in the foil. This observation is in contrast to regions away from the particles where the density of dislocations was quite low (Figs. 9(b)). It is clear from these observations that the low life sample had deformed non-uniformly with intense localized deformation confined mostly to the soft regions around the Hf-rich particles.

The misorientation of the subgrains in the soft region as calculated from the spacing of the dislocation network was found to be $\leq 4^{\circ}$. In regions close to the particle-matrix interface, e.g. region A in Fig. 11(a), SADP indicated that the misorientations were as high as 14° (Fig. 11(b)). In a thicker section of the foil where the particles were still intact, only one type of slip band was found to emanate from the Hf-rich particles, as shown by arrows in Fig. 12. The smaller Hf - rich particles (≤ 0.5 μm), typically observed in high life sample B-17, did not have such a strong effect on deformation, since they did not have a significant volume of soft region surrounding them. Prismatic dislocation loops decorated with G-phase precipitates were observed around these particles, as shown in Fig. 13.

Thus, it is clear that presence of large Hf-rich particles (> 0.5 μm) was largely responsible for changing the deformation behavior and degrading the creep rupture life in the low life specimens. Not only are these particles responsible for creating soft regions around the particles, they can also generate large stress gradients in the material. Finite element simulations have shown that under the action of an applied stress, the average von Mises stress distribution in a matrix with a reinforced particle changes considerably especially around and near the particle [15]. In the presence of a large number of particles with a range of sizes and arbitrary shapes, the stress distribution is quite complex and a function of several factors such as the particle aspect ratio, particle volume fraction, their orientation relative to the loading axis and with respect to each other [15]. Based on the results of these simulations it is suggested that if the Hf-rich particles are present in a specimen, they can play an important role in changing the local stress distribution,which would have been otherwise uniform. The localized stresses that develop near the particles can promote strong localized plastic deformation [16]. The soft regions produced by a lower density of G-phase precipitates

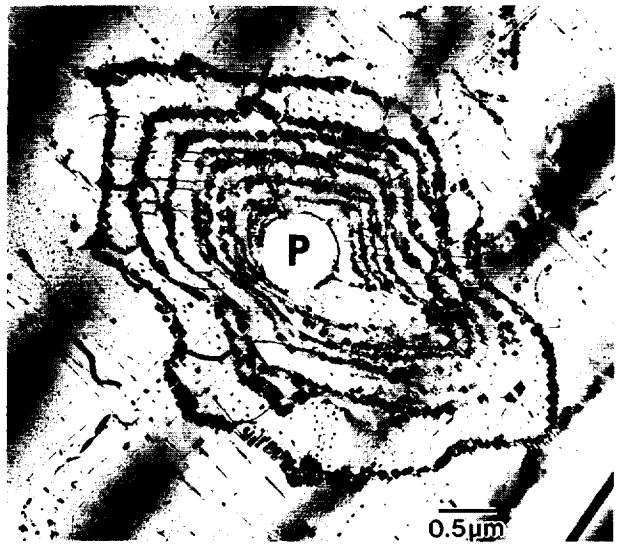

Fig. 13 Dislocation loops decorated by G-precipitates around an etched out Hf-rich particle (P) of size ~ 0.5 μm.

around the particles also help to accentuate this localized deformation. Recovery and recrystallization processes occurring in the soft regions can then produce large lattice rotations, which in turn can introduce enough local stresses to bias the deformation behavior from a duplex slip to a single slip mechanism. On the other hand, if the distribution of Hf-rich particles is such that high local stresses develop at or in the vicinity of the particles, a slip system totally different from <101>{101} could possibily be activated. Detailed dislocation analysis and computer modeling should further elucidate the problem.

Summary and Conclusions

The present study has demonstrated that the presence of large (> 0.5 μm) Hf-rich particles can have detrimental effect on the creep life of a Hf containing NiAl alloy. This effect arises due to two reasons. First, these particles deplete the surrounding matrix of Hf (and possibly Si), which in turn leads to a lower density of strengthening precipitates, thereby producing soft regions around the particles. Second, the presence of these particles sets up a non-uniform stress distribution in the material. Both these effects can result in localized deformation and consequently change the slip behavior from duplex to single slip.

Under identical homogenization conditions, the presence of Hf-rich particles in one ingot vs. another suggests that optimization of homogenization conditions is very important in these alloys. Minimization of the size and density of the Hf-rich particles is necessary in order to avoid scatter in the creep rupture life in Hf containing NiAl single crystal alloys.

Acknowledgements

The authors would like to acknowledge the help and valuable suggestions from several of their colleagues during various stages of this study. They are Randy Bowman, Bob Field, Ralph Garlic, Ivan Locci, Mike Nathal, Bob Miner, Ron Noebe, Scott Walston and Dan Whittenberger. Special thanks to Drs. Ron Noebe and Mike Nathal for reviewing the paper.

References

1. R. Darolia et al., "Overview of NiAl Alloys for High Temperature Applications,"Ordered Intermetallics - Physical Metallurgy and Mechanical Behavior (Dordecht, The Netherlands : Kluwer Academic Publishers, 1992), 679-698.

2. R. Darolia, "NiAl Alloys for High-Temperature Structural Applications," JOM, 43 (1991), 44-49.

3. R. Darolia, "NiAl for Turbine airfoil Applications," Structural Intermetallics, ed. R. Darolia et al. (Warrendale, PA: The Minerals, Metals and Materials Society, 1993), 495-504.

4. K. Vedula et al., "Alloys Based on NiAl for High Temperature Applications," High-Temperature Ordered Intermetallics Alloys, ed. C. C. Koch, C. T. Liu, and N. S. Stoloff (Materials Research Society, 1985), 411-421.

5. W. S. Walston et al., "Microstructure and High Temperature Strength of NiAl Alloys," Structural Intermetallics, ed. R. Darolia et al. (Warrendale, PA: The Minerals, Metals and Materials Society, 1993), 523-532.

6. I. E. Locci et al., "Microstructure and Mechanical Properties of a Single Crystal NiAl Alloy with Zr or Hf rich G-Phase Precipitates," High-Temperature Ordered Intermetallics Alloys IV, ed. L. Johnson, D. P. Pope, and J. O. Stiegler (Materials Research Society, 1991), 1013-1018.

7. M. Takeyama and C. T. Liu, "Microstructures and Mechanical Properties of NiAl-Ni_2AlHf Alloys," J. Mater. Res., 5 (1990), 1189-1196.

8. I. E. Locci et al., "Microstructure and Mechanical Properties of Cast, Homogenized and Aged NiAl Single Crystal containing Hf," High-Temperature Ordered Intermetallics Alloys V, ed. I. Baker et al., (Materials Research Society, (288), 1993), 685-690.

9. A. Garg, R. D. Noebe and R. Darolia, "Characterization of the Microstructure of Dilute Hf-Doped NiAl Single Crystal Alloys containing Si," Proceedings of the 8th Annual HITEMP Review-1995, (sponsored by NASA Lewis Research Center), To appear.

10. A. Garg, R. D. Noebe, and R. Darolia, " Crystallography of the NiHfSi Phase in a NiAl(0.5Hf) Single-Crystal Alloy," Acta Metall. Mater. (submitted).

11. F. C. Monkman and N. J. Grant, "An Empirical Relationship between Rupture Life and Minimum Creep Rate in Creep-Rupture Tests," Proc. ASTM, 56 (1956), 593-620.

12. A. Garg and R. D. Noebe, Unpublished Work, NASA Lewis Research Center, Cleveland OH.

13. K. R. Forbes et al., " High Temperature Deformation of Single Crystals of NiAl," High-Temperature Ordered Intermetallics Alloys V, ed. I. Baker et al., (Materials Research Society, (288), 1993), 45-57.

14. R. Darolia et al., " A Mechanistic Study of Microalloying Effects in NiAl" (AFOSR Contract Report, GEAE/ F49620-91-C-0077, GE Aircraft Engines, 1995).

15. Z. Wang, T. K. Chen, and D. J. Lloyd, " Stress Distribution in Particulate-Reinforced Metal-Matrix Composites Subjected to External Load," Metall. Trans., 24A (1993), 197-207.

16. J. G. Cowie and F. R. Tuler, " Flow Localization Models - A Review," Mater. Sci. Eng., 95 (1987), 93-99.